Title

Abnormal Myelin and Axonal Integrity in Recently Diagnosed Patients with Obstructive Sleep Apnea

Journal

Sleep, 37(4)

ISSN

0161-8105

Authors

Kumar, Rajesh
Pham, Tiffany T
Macey, Paul M
et al.

Publication Date

2014-04-01

DOI

10.5665/sleep.3578

Peer reviewed

http://dx.doi.org/10.5665/sleep.3578

Abnormal Myelin and Axonal Integrity in Recently Diagnosed Patients with Obstructive Sleep Apnea

Rajesh Kumar, PhD[1,2,6]; Tiffany T. Pham, BS[3]; Paul M. Macey, PhD[4,6]; Mary A. Woo, RN, DNSc[4]; Frisca L. Yan-Go, MD[5]; Ronald M. Harper, PhD[3,6]

[1]Department of Anesthesiology, [2]Department of Radiological Sciences, and [3]Department of Neurobiology, David Geffen School of Medicine at UCLA, Los Angeles, CA; [4]UCLA School of Nursing, Los Angeles, CA; [5]Department of Neurology, David Geffen School of Medicine at UCLA, Los Angeles, CA; [6]The Brain Research Institute, University of California at Los Angeles, Los Angeles, CA

Study Objectives: Patients with obstructive sleep apnea (OSA) show significant white matter injury; whether that injury represents myelin or axonal damage is unclear. The objective was to examine myelin and axonal changes in patients with newly diagnosed OSA over control subjects.

Design: Cross-sectional study.

Setting: University-based medical center.

Participants: Twenty-three newly-diagnosed, treatment-naïve OSA and 23 age- and sex-matched control subjects.

Interventions: None.

Measurements and Results: Radial and axial diffusivity maps, calculated from diffusion tensor imaging data (3.0 Tesla MRI scanner), indicating diffusion perpendicular (myelin status) or parallel (axonal status) to fibers, respectively, were normalized, smoothed, and compared between groups (analysis of covariance; covariate: age). Global brain radial and axial diffusivity values, and global brain volume with myelin and axonal changes were determined, and region-of-interest analyses performed in areas of significant differences between groups based on voxel-based procedures. Global radial and axial diffusivity values were significantly reduced in OSA versus control subjects (radial, $P = 0.004$; axial, $P = 0.019$), with radial (myelin) diffusivity reduced more than axial (axonal), and more left-sided reduction for both measures. Localized declines for myelin and axonal measures appeared in the dorsal and ventral medulla, cerebellar cortex and deep nuclei, basal ganglia, hippocampus, amygdala, corpus callosum, insula, cingulate and medial frontal cortices, and other cortical areas ($P < 0.005$), all regions mediating functions affected in OSA.

Conclusions: Fiber injury appears in critical medullary respiratory regulatory sites, as well as cognitive and autonomic control areas. Myelin is more affected in newly diagnosed OSA than axons, and primarily on the left side, possibly from the increased myelin sensitivity to hypoxia and asymmetric perfusion.

Keywords: Acute, brain, diffusion, hypoxia, medulla, respiration, tensor imaging

Citation: Kumar R; Pham TT; Macey PM; Woo MA; Yan-Go FL; Harper RM. Abnormal myelin and axonal integrity in recently diagnosed patients with obstructive sleep apnea. *SLEEP* 2014;37(4):723-732.

INTRODUCTION

Patients with obstructive sleep apnea show regional white and gray matter abnormalities in multiple brain sites, as determined by diffusion tensor imaging (DTI)-based fractional anisotropy and mean diffusivity,[1,2] and voxel-based morphometry procedures using high-resolution T1-weighted images.[3-6] Brain regions with injury in OSA appear in medullary, cerebellar, basal ganglia, and limbic areas that regulate autonomic, cognitive, and mood functions,[1-6] all of which are deficient in the condition, and may contribute substantially to the comorbidities accompanying the syndrome. Whether white matter injury in newly diagnosed, treatment-naïve OSA subjects reflects predominantly myelin or axonal changes is unknown, but determining the type of injury is essential for interventions against further damage, and such determination was the objective of the studies here.

A principal characteristic of OSA is exposure to periods of sustained intermittent hypoxia. Myelin is more sensitive to hypoxia than neural tissue,[7] suggesting that myelin would have a lower threshold for injury in the syndrome than axons; however, such a finding has not been documented. Moreover, the duration of hypoxic exposure is of interest in injury determination. Presumably, very long exposure to low oxygen would target both myelin and axons. The need to determine the type of white matter injury, myelin versus axonal, thus requires evaluation at a time of minimal hypoxic exposure, and for that reason, we chose to examine newly diagnosed OSA subjects, untreated with ventilatory support or other means during sleep.

Magnetic resonance imaging (MRI) procedures can determine white matter composition non-invasively. DTI-based radial diffusivity (which measures water diffusion perpendicular to axons) preferentially indicates myelin changes and axial diffusivity (which examines water diffusion parallel to axons), primarily shows axonal changes,[8-12] and can assist evaluation of tissue characteristics. Both procedures offer sensitive means to examine subtle tissue alterations and provide pathological information (myelin versus axonal changes). These procedures have been used successfully for pathological fiber determination in other brain conditions including multiple sclerosis,[13] Alzheimer disease,[14] traumatic brain injury,[15] new-onset seizures,[16] and brain developmental and aging conditions,[17,18] and offer promise in evaluating tissue pathology in OSA.

The sensitivity of radial and axial diffusivity techniques also offers substantial benefits for detecting injury in OSA, especially in medullary and midbrain areas where volumetric procedures examining tissue loss have been unable to determine local damage in the condition.[3] Medullary regions contain

Submitted for publication July, 2013
Submitted in final revised form October, 2013
Accepted for publication October, 2013

Address correspondence to: Rajesh Kumar, PhD, Department of Anesthesiology, David Geffen School of Medicine at UCLA, University of California at Los Angeles, Los Angeles, CA 90095-1763; Tel: (310) 206-1679, 6133; Fax: (310) 825-2236; E-mail: rkumar@mednet.ucla.edu

essential sensory and motor regulatory sites for breathing and sympathetic control; although medullary injury has been suspected because of the exaggerated sympathetic tone to the musculature[19] and the failure to activate upper airway muscles in temporal congruence with the diaphragm during sleep, such potential damage has not been assessed adequately.

Here, we examined global and regional brain axial and radial diffusivity changes in newly diagnosed, treatment-naïve OSA, relative to age- and sex-matched control subjects. Because OSA subjects showed either gray matter volume loss or tissue changes in medullary, cerebellar, basal ganglia, and limbic areas in previous studies,[2-6,17] we hypothesized that global measures of myelin and axonal changes (axial and radial diffusivity values) would be reduced in recently diagnosed OSA subjects, compared to controls, as a consequence of the acute nature of the pathology, and that regional declines would appear in and between the brain areas found earlier to have been injured in the syndrome.[1-3] The patterns of injury may differ from those with very long-term exposure to OSA, but the incentive to find appropriate interventions mandates the need to describe the nature of changes as early as possible in the syndrome.

METHODS

Design

We used a comparative cross-sectional design to examine types of brain white matter injury in recently diagnosed, treatment-naïve subjects with OSA over control subjects.

Subjects

Twenty-three OSA and 23 age- and sex-matched healthy control subjects were studied. Additional OSA and control subjects were studied, but a scanner upgrade in the midst of acquisition from those subjects had the potential to alter signal characteristics; thus, we included only data collected from the same scanner platform with identical data acquisition parameters. All OSA subjects were recently diagnosed via overnight polysomnography (apnea-hypopnea index $\geq$ 15), treatment-naïve, and recruited from the sleep disorders laboratory at the UCLA Medical Center. OSA subjects were without any medications, such as β-blockers, α-agonists, angiotension-converting enzyme inhibitors, vasodilators, or mood-altering drugs (e.g., serotonin reuptake inhibitors). Other exclusion criteria for both OSA and control subjects included history of stroke, heart failure, diagnosed conditions that may affect the brain, non magnetic resonance imaging (MRI)-compatible metallic implants, or body weight more than 125 kg. For all subjects, weight was chosen as an exclusion criterion over body mass index (BMI) due to MRI scanner table limitations. Control subjects were healthy, recruited specifically for this study, without any disorder that might alter brain tissue, had no evidence of sleep disorders, and were recruited from the Southern California region. All subjects provided written and informed consent before the study, and the study protocol was approved by the Institutional Review Board at University of California at Los Angeles.

Assessment of Daytime Sleepiness and Sleep Quality

OSA and control subjects were examined for daytime sleepiness with the Epworth Sleepiness Scale (ESS), and sleep quality with the Pittsburg Sleep Quality Index (PSQI) questionnaires.[20] Both of these commonly used daytime sleepiness and sleep quality questionnaires were administered only once to all subjects immediately before or after MRI data acquisition.

Magnetic Resonance Imaging

Brain imaging studies were performed using a 3.0-Tesla MRI scanner (Siemens, Magnetom Tim-Trio, Erlangen, Germany), with a receive-only eight-channel phased array head coil and a whole-body transmitter coil. Foam pads were used on both sides of the head to minimize head motion during data acquisition. High-resolution T1-weighted images were acquired using a magnetization prepared rapid acquisition gradient-echo pulse sequence [repetition time (TR) = 2200 ms; echo time (TE) = 2.2 ms; inversion time = 900 ms; flip angle = 9°; matrix size = 256 × 256; field of view (FOV) = 230 × 230 mm; slice thickness = 1.0 mm]. Proton density (PD) and T2-weighted scans were collected simultaneously in the axial plane, using a dual-echo turbo spin-echo pulse sequence (TR = 10,000 ms; TE1, 2 = 17, 134 ms; flip angle = 130°; matrix size = 256 × 256; FOV = 230 × 230 mm; slice thickness = 4.0 mm). DTI data were collected using a single-shot echo planer imaging with twice-refocused spin-echo pulse sequence (TR = 10,000 ms; TE = 87 ms; flip-angle = 90°; band width = 1,346 Hz/pixel; matrix size = 128 × 128; FOV = 230 × 230 mm; slice thickness = 2.0 mm, diffusion values = 0 and 700 s/mm^2, diffusion directions = 12, separate series = 4). The parallel imaging technique, generalized autocalibrating partially parallel acquisition, with an acceleration factor of two was used in all scans for MRI data acquisition.

Data Processing and Analyses

We used the statistical parametric mapping package SPM8 (http://www.fil.ion.ucl.ac.uk/spm/), DTI-Studio (v3.0.1),[21] MRIcroN, and MATLAB-based (http://www.mathworks.com/) custom software to preprocess and analyze data.

High-resolution T1-weighted, PD- and T2-weighted images were used to assess any visible brain tissue abnormalities such as infarcts, tumors, cysts, or any other major mass lesion in OSA and control subjects. We also examined diffusion- and nondiffusion-weighted images of OSA and control subjects for any head motion-related or other imaging artifacts prior to radial and axial diffusion calculation. All OSA and controls subjects included in this study showed no other major visible brain injury, head motion, or other imaging artifacts that could affect radial and axial diffusion measures.

Radial and Axial Diffusivity Calculation

The average background noise level from outside the brain tissue was calculated using non-diffusion and diffusion-weighted images, and was used to suppress nonbrain areas in OSA and control subjects during radial and axial diffusivity calculations. Using diffusion-weighted (b = 700 s/mm^2) and nondiffusion-weighted images (b = 0 s/mm^2), diffusion tensor matrices were calculated and diagonalized, and principal eigenvalues (λ1, λ2, and λ3) were determined using DTI-Studio software.[21] The principal eigenvalues were used to calculate radial [$\lambda_\perp = (\lambda 2 + \lambda 3)/2$] and axial ($\lambda_\parallel = \lambda 1$)

diffusivity values at each voxel, with voxel intensities on the radial and axial diffusivity maps showing the corresponding radial and axial values.[8-12]

Realignment, Averaging, Normalization, and Smoothing of Radial and Axial Diffusion Maps

The radial and axial diffusivity maps, derived from each DTI series, were realigned to remove any potential variation from head motion and averaged to create one radial and axial diffusivity map per subject. Similarly, nondiffusion-weighted images were also realigned and averaged.

The realigned and averaged radial and axial diffusivity maps were normalized to Montreal Neurological Institute (MNI) space. For normalization of radial and axial diffusivity maps, non-diffusion-weighted (b0) images were normalized to MNI space using a unified segmentation approach,[22] and resulting normalization parameters were applied to corresponding radial and axial diffusivity maps, b0 images, and gray and white matter probability maps. The normalized radial and axial diffusivity maps were smoothed with a Gaussian filter (10 mm).

Background Images

High-resolution T1-weighted images of all OSA and control subjects were segmented into gray, white, and cerebrospinal fluid (CSF) tissue types, based on a *priori*-defined distributions of gray, white, and CSF using unified segmentation procedure.[22] The normalization parameters resulting from the segmentation step were applied to corresponding T1-weighted images of individuals. The normalized T1-weighted images of OSA and control subjects were averaged to derive whole-brain mean images (background images), and were used for structural identification.

Global Brain Mask

We averaged the normalized white matter probability maps derived from b0 images of OSA and control subjects. Similarly, gray matter probability maps derived from b0 images of OSA and control subjects were averaged. We thresholded (white matter probability > 0.3; gray matter probability > 0.3) and combined the averaged gray and white matter probability maps to determine a global brain mask.

Calculation of Global Brain Radial and Axial Diffusivity Values

We removed CSF and other nonbrain regions from the normalized radial and axial diffusivity maps using a global brain mask, derived from all OSA and control subjects. The masked radial and axial diffusivity maps were used to determine mean global brain radial and axial diffusivity values using MATLAB-based custom software.

Region-of-Interest Analysis

Region-of-interest (ROI) analyses were used to calculate average radial and axial diffusivity values from those brain sites that show significant changes in myelin and axonal integrity between OSA and control groups, based on whole-brain voxel-by-voxel analysis. Regional ROI masks were created for brain sites using clusters determined by voxel-by-voxel analysis procedures, and used to determine average radial and axial diffusivity values of those areas from OSA and control individuals using normalized and smoothed radial and axial diffusivity maps.

Calculation of Global Brain Volume With Myelin and Axonal Changes

Brain volumes with significant myelin and axonal changes were calculated using statistical parametric maps, derived from comparisons between OSA and control subjects for radial and axial diffusivity. The number of voxels in the statistical parametric maps related to radial or axial diffusivity changes were counted, and multiplied with the voxel volume.

Statistical Analysis

We used the Statistical Package for the Social Sciences (SPSS, V 18.0, IBM, Chicago, IL) software to examine demographic, biophysical, and sleep variables, and global brain radial and axial diffusivity values. The independent samples *t*-tests were performed to examine age, BMI, and sleep variables differences between OSA and control groups. Global brain radial and axial diffusivity values were assessed between OSA and control groups using analysis of covariance (ANCOVA; covariate: age). Significance levels were set at $P < 0.05$ for the statistical tests.

The normalized and smoothed radial and axial diffusivity maps were compared voxel by voxel between OSA and control subjects using ANCOVA (SPM8; covariate, age; uncorrected threshold, $P < 0.005$). Clusters with significant differences in myelin and axonal measures in brain areas between OSA and control subjects were overlaid onto background images for structural recognition. The percentage brain volume with myelin changes in OSA subjects was also calculated against brain volume with axonal changes.

The average radial and axial diffusivity values from ROI analyses of those regions that showed significant differences between groups were tabulated for magnitude differences, and were compared between OSA and control subjects with multivariate ANCOVA (covariate: age).

RESULTS

Demographics, Biophysical, and Sleep Variables

The demographic, biophysical, and sleep related variables are tabulated in Table 1. No significant differences in age ($P = 0.8$) was shown between OSA and control subjects. However, BMIs were significantly higher in OSA compared to control subjects ($P = 0.007$). Both ESS and PSQI showed significant differences between OSA and control subjects (ESS, $P = 0.001$; PSQI, $P < 0.001$).

Global Brain Radial and Axial Diffusivity Changes

The global brain radial diffusivity of OSA subjects was $0.69 \pm 0.03 \times 10^{-3}$ mm^2/s, and for controls was $0.72 \pm 0.04 \times 10^{-3}$ mm^2/s. The global brain axial diffusivity of OSA was $1.27 \pm 0.04 \times 10^{-3}$ mm^2/s, and for control subjects was $1.31 \pm 0.06 \times 10^{-3}$ mm^2/s. Both global brain radial (measure of myelin integrity) and axial (measure of axonal integrity) diffusivity values were significantly reduced in OSA over controls (radial diffusivity, $P = 0.004$; axial diffusivity, $P = 0.019$).

Table 1—Demographic, physiologic, and sleep variables of obstructive sleep apnea and control subjects

Variables	OSA (n = 23)	Controls (n = 23)	P value
Age range (y)	31-62	31-64	–
Age (mean ± SD, y)	44.4 ± 9.3	45.3 ± 11.0	0.8
Sex (Male:Female)	20:3	20:3	1.0
BMI (mean ± SD, kg/m^2)	30.1 ± 5.4	26.2 ± 3.7	0.007
Handedness	3 Left; 18 Right; 2 Ambidextrous	4 Left; 18 Right; 1 Ambidextrous	–
Ethnicity	7 Asian; 10 White; 3 Hispanic; 2 African-American; 1 Asian-White	4 Asian; 16 White; 3 Hispanic	–
AHI (mean ± SD, events/h)	34.9 ± 24.1	–	–
OSA severity	13 Moderate; 10 Severe	–	–
ESS (mean ± SD)	9.6 ± 5.5	4.7 ± 4.0	0.001
PSQI (mean ± SD)	8.3 ± 3.6	3.1 ± 1.7	< 0.001

AHI, apnea-hypopnea index; BMI, body mass index; ESS, Epworth Sleepiness Scale; OSA, obstructive sleep apnea; PSQI, Pittsburg Sleep Quality Index; SD, standard deviation.

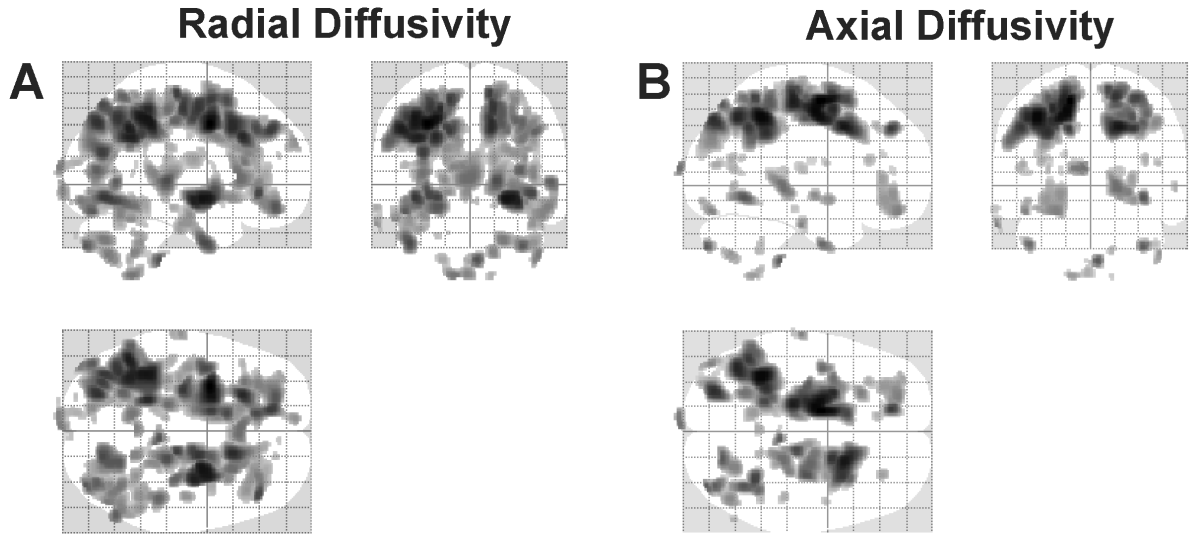

Figure 1—Brain sites showing significant radial (myelin) and axial (axonal) diffusivity changes in obstructive sleep apnea (OSA) (n = 23), compared to control (n = 23) subjects (uncorrected threshold, P = 0.005), displayed in glass brain mode with three-dimensional representations projected onto two-dimensional axial, sagittal, and coronal sections. **(A)** Brain areas with significantly reduced radial diffusivity values in OSA over control subjects. **(B)** Regions with reduced axial diffusivity in OSA compared to control subjects.

Brain Volume with Myelin and Axonal Changes

Global radial and axial values, as viewed on glass brain images, are shown in Figure 1. The summed volume of myelin changes in OSA, as shown as dark areas in the glass brain image, was 115911.0 mm^3, whereas the summed volume of axonal changes was 68,735.3 mm^3. Myelin changes were more widespread in OSA subjects than axonal changes (Figure 1A versus 1B); with 68% more volume with myelin changes over axonal changes. There was greater reduction of both axial and radial values on the left side (Figure 1A and 1B; left versus right; radial: 70,449.8 versus 45,461.3 mm^3, axial; 45,113.6 versus 23,621.6 mm^3).

Regional Voxel-by-Voxel Radial and Axial Diffusivity Changes

The ventrolateral medulla showed both radial and axial diffusivity reductions (myelin and axonal changes); myelin injury encompassed a relatively large area, extending from the caudal pons to 13 mm caudally (Figure 2, a and Figure 3, g), as identified by radial diffusivity, and axonal injury extended from the lateral border of the medulla to the midline, as shown by axial diffusivity (Figure 3, g). There was widespread reduction of myelin in cortical projections, the corona radiata from frontal regions to the occipital cortex (Figure 2, d-g, k), and included the left anterior and posterior insular (Figure 2, h and i), anterior and mid corpus callosum (Figure 2, b and c), dorsal and ventral temporal (Figure 2, u and v), and left mid and posterior cingulum bundle (Figure 2, o and p), as well as the bilateral anterior thalamus (Figure 2, q), superior cerebellar peduncles (Figure 2, w) and cerebellar cortex (Figure 2, r, x, y, and n). Myelin loss also appeared in the ventral hippocampus (Figure 2, j), and fibers within the right mid hippocampus extending to the retrolenticular internal capsule (Figure 2, l), right amygdala (Figure 2, m), posterior thalamus (Figure 2, t), and putamen and globus pallidus (Figure 2, s). Brain sites that showed axonal changes (reduced axial diffusivity) in OSA emerged

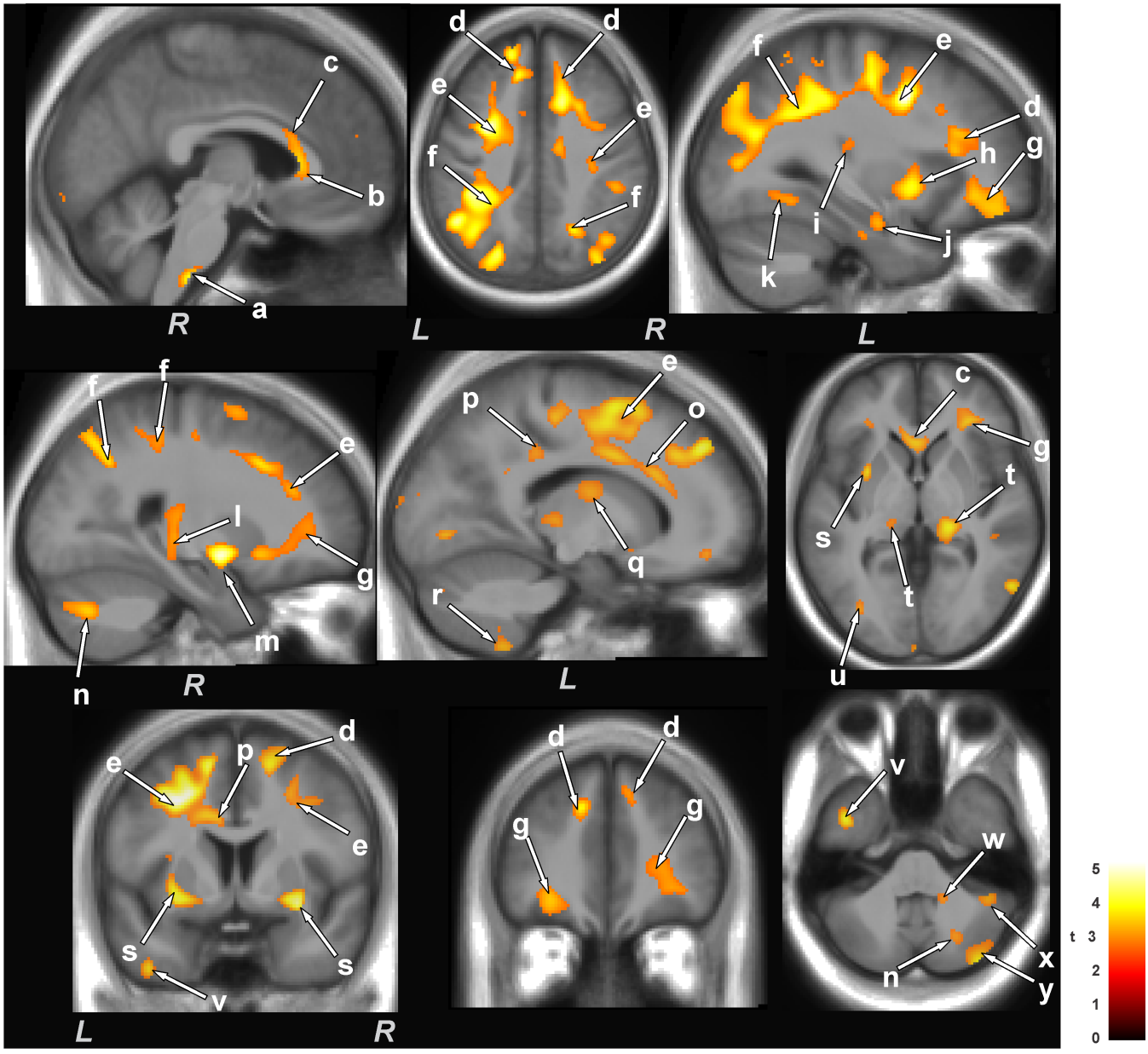

Figure 2—Brain regions with significantly reduced radial diffusivity (i.e., primarily myelin changes) in OSA compared to control subjects. Sites with reduced radial diffusivity in OSA included the ventrolateral medulla (a), corpus callosum (b,c), corona radiata (d-f), frontal white matter (g), insular cortices (h, i), ventral hippocampus (j), occipital white matter (k), mid hippocampus extending to the retrolenticular internal capsule (l), amygdala (m), cingulum bundle (o, p), dorsal and posterior thalamus (q, t), putamen and external capsules (s), temporal white matter (u), ventral temporal cortex (v), and cerebellar peduncles (w) and cerebellar cortices (n, r, x, y). All brain images are in neurological convention (L = left, R = right), and the color scale indicates t-statistic values.

in bilateral anterior (Figure 3, a), superior (Figure 3, b), and posterior (Figure 3, c) corona radiata, bilateral frontal white matter (Figure 3, d), bilateral globus pallidus (Figure 3, e), right posterior thalamus, extending to the hippocampus (Figure 3, f), dorsal and ventral temporal white matter (Figure 3, h and i), right putamen (Figure 3, j), right mid and posterior cingulate cortices (Figure 3, k and l), posterior corpus callosum (Figure 3, m), left posterior external capsule (Figure 3, n), and right cerebellar cortices (Figure 3, o).

ROI Analyses

The regional radial and axial diffusivity values derived from multiple brain regions from OSA and control subjects are tabulated in Tables 2 and 3. Radial and axial diffusivity values were significantly reduced in OSA over control subjects, consistent with the voxel-based analysis findings.

DISCUSSION

Overview

Both axons and their surrounding myelin are damaged in recently diagnosed, untreated OSA subjects, as indicated by significantly reduced global and regional radial and axial diffusivity. The injury was not uniformly distributed; more myelin changes appeared over axonal changes, and more damage was found on the left side for both myelin and axonal measures.

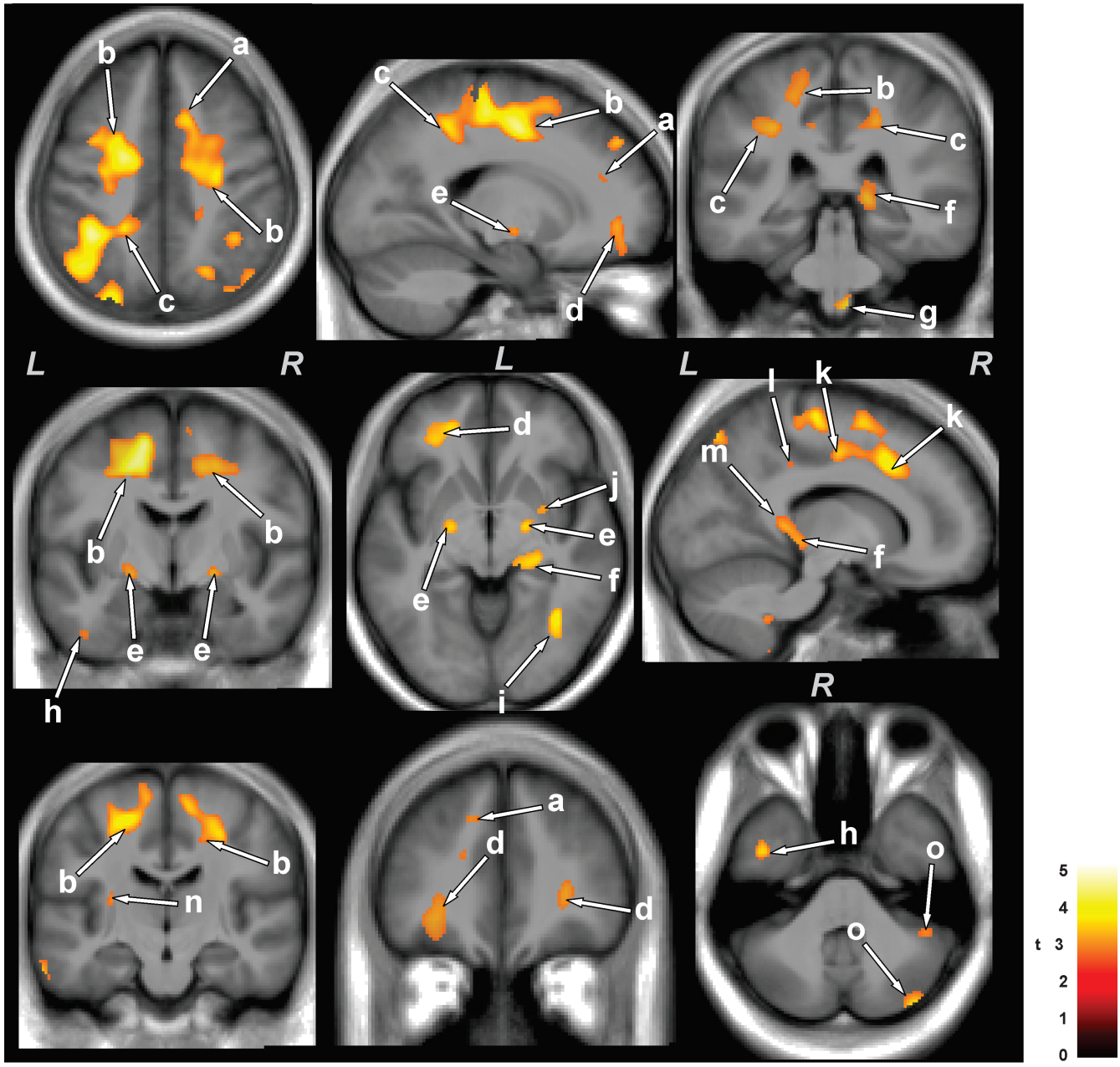

Figure 3—Brain areas with reduced axial diffusivity (i.e., largely axonal injury) in obstructive sleep apnea (OSA) over control subjects. Areas with reduced axial diffusivity in OSA compared to control subjects included the corona radiata (a-c), frontal white matter (d), globus pallidus (e), thalamus, extending to the hippocampus (f), ventral medulla (g), temporal white matter (h, i), putamen (j), cingulate cortices (k, l), corpus callosum (m), external capsule (n), and cerebellar cortices (o). Figure conventions are the same as in Figure 2.

Of substantial importance for the syndrome, a large area of the ventrolateral medulla, extending from the caudal pons for 13 mm caudally and including at its widest area, tissue from the lateral edge to the midline showed injury, a region incorporating major components of respiratory control and sympathetic regulation. In addition, damage appeared in cerebellar cortex, important for blood pressure and respiratory muscle coordination, as well as fibers of the basal ganglia, hippocampus, and amygdala, mediating cognitive, memory, and autonomic aspects. Widespread projections to the cortex, as well as insular and cingulate fibers, important for affect and autonomic regulation, also showed myelin injury. The ratio of myelin to axonal injury suggests that acute influences from hypoxia likely underlie the damage in newly diagnosed OSA subjects.

Assessment of Myelin and Axonal Injury

Radial diffusivity, which measures water diffusion perpendicular to fibers, and axial diffusivity that assesses water diffusion parallel to fibers can be used to differentiate types of white matter pathologies.[11,12] The directional nature of radial and axial diffusivity measures in white matter can show myelin status by radial diffusivity indices, with axial diffusivity principally indicating axonal changes.[11,12] Radial diffusivity is modified by alterations in myelin, including myelin sheath permeability and

Table 2—Average radial diffusivity values ($\times 10^{-6}$ mm^2/s) of multiple brain regions from obstructive sleep apnea and control subjects

Brain regions	Radial diffusivity		[A] vs [B]	Figures
	OSA (Mean ± SD) [A]	Control (Mean ± SD) [B]	P values	
R ventrolateral medulla	1731.57 ± 218.24	1924.97 ± 148.85	0.001	Figure 2, a
R anterior corpus callosum	973.30 ± 110.13	1101.38 ± 164.49	0.003	Figure 2, b
R mid corpus callosum	944.68 ± 99.47	1066.99 ± 147.75	0.002	Figure 2, c
L superior corona radiata	693.63 ± 53.17	756.62 ± 83.34	0.001	Figure 2, d
R superior corona radiata	619.43 ± 37.63	664.45 ± 48.84	0.000	Figure 2, d
L mid corona radiata	592.30 ± 36.77	633.39 ± 40.07	0.000	Figure 2, e
R mid corona radiata	640.33 ± 40.92	678.42 ± 43.08	0.001	Figure 2, e
L posterior corona radiata	688.76 ± 36.81	730.24 ± 51.52	0.000	Figure 2, f
R posterior corona radiata	710.20 ± 41.25	763.23 ± 62.76	0.001	Figure 2, f
L frontal white matter	694.78 ± 38.07	739.90 ± 66.10	0.002	Figure 2, g
L anterior insular cortex	735.36 ± 35.74	774.40 ± 49.38	0.002	Figure 2, h
L posterior insular cortex	677.87 ± 45.74	728.09 ± 71.34	0.006	Figure 2, i
L ventral hippocampus	865.08 ± 56.36	938.24 ± 97.39	0.004	Figure 2, j
L occipital white matter	621.05 ± 35.90	657.78 ± 31.65	0.000	Figure 2, k
R mid hippocampus	936.02 ± 136.05	1049.33 ± 148.58	0.007	Figure 2, l
R retrolenticular internal capsule	729.05 ± 66.01	806.56 ± 83.55	0.001	Figure 2, l
R amygdala	765.30 ± 45.51	821.59 ± 57.01	0.000	Figure 2, m
R cerebellar cortex	638.20 ± 41.06	687.35 ± 61.42	0.003	Figure 2, n
L cingulum bundle	612.86 ± 39.76	665.22 ± 66.47	0.001	Figure 2, o
L cingulum bundle	698.59 ± 34.42	730.97 ± 49.99	0.005	Figure 2, p
L anterior thalamus	874.57 ± 116.86	986.97 ± 155.27	0.006	Figure 2, q
L cerebellar cortex	1088.02 ± 160.87	1225.46 ± 123.48	0.003	Figure 2, r
L external capsule	706.97 ± 33.73	743.32 ± 40.79	0.001	Figure 2, s
L putamen	656.47 ± 35.50	687.99 ± 27.04	0.002	Figure 2, s
L posterior thalamus	651.84 ± 70.14	707.55 ± 53.91	0.004	Figure 2, t
R posterior thalamus	867.77 ± 99.75	962.82 ± 87.84	0.001	Figure 2, t
L temporal white matter	599.12 ± 30.74	626.50 ± 28.78	0.004	Figure 2, u
L ventral temporal cortex	804.86 ± 78.02	884.12 ± 85.89	0.002	Figure 2, v
R superior cerebellar peduncles	718.80 ± 76.95	780.72 ± 58.52	0.003	Figure 2, w
R cerebellar cortex	1025.75 ± 142.34	1183.06 ± 210.94	0.004	Figure 2, x
R cerebellar cortex	704.17 ± 72.33	794.45 ± 109.50	0.002	Figure 2, y

L, left; OSA, obstructive sleep apnea; R, right; SD, standard deviation.

packing characteristics.[23,24] However, axial diffusivity is influenced by axonal density, caliber, straightness of axons, extra-axonal/extracellular space, and focal enlargement/constriction of neuritis (beading)[25,26]; any change in these tissue characteristics can alter axial diffusivity.

Effect of Multiple Hypoxic Episodes on Acute Stages

The principal characteristic of OSA, cessation of air movement through repeated airway obstructions with continued diaphragmatic efforts during sleep, leads to successive exposures to intermittent hypoxia with subsequent reoxygenation when breathing resumes. The mismatch of oxygen demand and supply to brain tissue results in alterations in sodium and potassium ions in extracellular and intracellular space.[27-29] Such changes in sodium and potassium channels alter intracellular and extracellular water, and result in cell and axonal swelling.[30] Other changes include excessive glutamate release that also contributes to tissue injury.[31] The affected glial cells, neurons, and myelin-supporting oligodendrocytes cells all play essential roles in axonal function and survival,[32-34] and are highly sensitive to hypoxia. The hypoxic exposure can lead to myelin and axonal swelling, and decreased extracellular/extra-axonal space.

In acute hypoxic stages, axonal inflammation, which decreases extra-axonal space, as well as water reduces axial diffusivity due to reduced water diffusion parallel to fibers. Myelin swelling in the acute stage contributes to slowing of water motion perpendicular to fibers, reducing radial diffusivity. Both radial and axial diffusivity values decline in acute pathological stages of hypoxia and ischemia conditions, indicating myelin and axonal alterations, respectively.[33,35,36]

Asymmetric Injury: Implications for Function

Global myelin and axonal changes preferentially appeared on the left side, although, as Figure 1 demonstrates, injury emerged bilaterally. The lateralization of injury follows a pattern of gray matter damage found in a number of regional areas in OSA.[1,3] The mechanisms underlying the asymmetry are unclear, but likely rest on relative perfusion differences

Table 3—Mean axial diffusivity values ($\times 10^{-6}$ mm^2/s) of various brain sites from obstructive sleep apnea and control subjects

	Axial diffusivity			
Brain regions	**OSA (Mean ± SD) [A]**	**Control (Mean ± SD) [B]**	**[A] vs [B] P values**	**Figures**
L superior corona radiata	1171.99 ± 30.29	1213.27 ± 72.01	0.009	Figure 3, a
R superior corona radiata	1205.91 ± 40.48	1259.73 ± 79.74	0.003	Figure 3, a
L mid corona radiata	1218.13 ± 31.45	1266.36 ± 47.70	0.000	Figure 3, b
R mid corona radiata	1224.96 ± 36.89	1276.30 ± 55.68	0.000	Figure 3, b
L posterior corona radiata	1354.97 ± 55.96	1413.37 ± 78.76	0.001	Figure 3, c
L frontal white matter	1207.53 ± 29.79	1250.76 ± 64.08	0.003	Figure 3, d
R frontal white matter	1170.71 ± 35.97	1208.57 ± 56.28	0.005	Figure 3, d
L globus pallidus	1339.76 ± 55.79	1385.74 ± 44.67	0.004	Figure 3, e
R hippocampus	1712.85 ± 171.16	1852.77 ± 175.99	0.006	Figure 3, f
R posterior thalamus	1800.60 ± 161.97	1965.03 ± 166.76	0.001	Figure 3, f
R ventrolateral medulla	2561.79 ± 224.70	2744.71 ± 158.08	0.003	Figure 3, g
L temporal white matter	1224.71 ± 47.64	1276.71 ± 56.43	0.002	Figure 3, h
R temporal white matter	1165.82 ± 46.19	1207.90 ± 35.80	0.001	Figure 3, i
R putamen	1196.14 ± 44.71	1243.21 ± 72.01	0.005	Figure 3, j
R mid cingulate cortex	1227.91 ± 50.75	1309.62 ± 79.74	0.000	Figure 3, k
R mid cingulate cortex	1338.75 ± 77.54	1398.89 ± 47.70	0.006	Figure 3, l
R posterior corpus callosum	1989.78 ± 161.90	2152.23 ± 55.68	0.004	Figure 3, m
L external capsule	1261.79 ± 38.11	1302.47 ± 78.76	0.007	Figure 3, n
R cerebellar cortices	1311.87 ± 125.70	1472.58 ± 64.08	0.001	Figure 3, o

L, Left; OSA, obstructive sleep apnea; R, right; SD, standard deviation.

between the left and right brain. Asymmetrical injury to white matter in watershed areas shows a very high correlation with cerebrovascular insufficiency.[37]

The asymmetry of damage is reflected in functional impairments from structures showing gray matter injury in OSA, and in other sleep disordered breathing conditions of heart failure and congenital central hypoventilation syndrome.[2,3,8-10] The lateralized injury to fibers in the ventrolateral medulla poses a special concern for cardiovascular control, because on the right side injury could result in enhanced asymmetrical sympathetic discharge, which has the potential to introduce serious cardiac arrhythmia[38]; a range of arrhythmia, including atrial fibrillation, is frequently found in OSA.[39]

Altered Regional Myelin, Axonal Integrity, and Functional Deficits

Multiple brain areas show reduced gray matter volume, white matter damage, and metabolic abnormalities in OSA subjects.[1-3,5,6,40] Those brain areas principally are located in rostral brain and cerebellar regions, are often lateralized, and are typically associated with autonomic, memory, and cognitive regulation. The cortical areas include medial prefrontal, insular, and cingulate cortices, all involved in affective disorders including depression and anxiety,[41,42] and with autonomic regulation, especially of the sympathetic system. Subcortical structures showing injury were also present in more rostral areas, and include the hippocampal memory system with its mammillary bodies, anterior thalamic projections, cognitive areas including the basal ganglia, and sensory integrative areas of the thalamus.[1,3,40] White matter injury was demonstrated by fractional anisotropy techniques, and showed loss of fiber integrity in the anterior cingulate, fornix, cerebellar projection areas, corpus callosum, and multiple cortical projection areas.[2] The current study extends those findings of loss of fiber integrity to show the nature of fiber damage and shows the loss of axons and myelin injury, and does so in early stages of the syndrome without concern about potential repair of tissue with continuous positive airway pressure or other intervention.

The right ventrolateral medulla (VLM) showed significant damage; this injury covered a substantial area that included the region incorporating the retrotrapezoid nuclei, pre-Botzinger nucleus, as well as the rostral and caudal ventrolateral nuclei. The retrotrapezoid nuclei play significant roles in CO_2 integration with respiratory patterns,[43] and the pre-Botzinger nuclei serve major patterning roles.[44] The caudal and rostral VLM are essential to integrate sympathetic regulation, and form the final output pathway for sympathetic outflow to the intermediolateral column of the spinal cord, with the caudal VLM receiving afferents and integration those signals for that control.[45,46]

The finding of injury in this ventrolateral medullary site significantly expands the field of potential mechanisms that may be operating to create or continue the processes underlying mechanisms of OSA. The characteristic feature of OSA is loss of discharge of upper airway muscles with continued, often exaggerated diaphragmatic and abdominal respiratory musculature. The loss of drive to upper airway musculature has been a subject of considerable attention, with speculation of failed neurotransmitter action,[47] or distorted timing of blood pressure elevation integration on the respiratory musculature.[48] The ventrolateral medullary injury provides a focus for attention to be directed toward sites classically associated with respiratory patterning.

The damage to the rostral and caudal VLM also directs attention to the enhanced sympathetic tone in OSA, and the relatively invariant poor responsivity of the sympathetic system to sensory input in the condition.[49] The two medullary nuclei serve essential integrative and output roles for the sympathetic system.[49] Those nuclei are damaged in other sleep disordered breathing conditions, such as congenital central hypoventilation syndrome and heart failure,[8,10] and show lateralized, impaired responses to Valsalva pressor maneuvers.[50-52] The lateralized medullary damage in OSA, combined with the largely unilateral insular injury shown earlier provides a framework for asymmetric autonomic nervous system action.

Injury also appeared on the caudate, hippocampus, putamen, cerebellum, cingulate cortex, cingulum bundle, and corpus callosum, brain sites that are involved in cognitive regulation, affect, and language transfer, functions that are deficient in OSA subjects. Other abnormal brain function in OSA includes mood regulation, and sites that control such function, including the cingulate and insular cortices, and hippocampus, and are also injured in the condition.

Limitations

Multiple limitations of this study should be acknowledged, and include inadequate data contributions from females and the absence of precise disease duration data from OSA subjects. Data from only a limited number of females were available, and the nature and pattern of injury may differ in newly diagnosed females with OSA over males, because gray matter and fiber integrity differ between male and female OSA subjects.[53]

OSA subjects included in this study were recently diagnosed; however, disease duration may be variable because of multiple issues that may have delayed identification and assessment of the condition. However, both global and regional radial and axial diffusivity showed reduced values, indicating an acute disease condition; thus, we believe that most OSA subjects were in an acute stage of chronic tissue injury.

None of the subjects was exposed to any treatment modality before MRI assessment. Thus, the possibility of interventions for the syndrome altering the outcomes can be ruled out.

CONCLUSIONS

Global brain measures of myelin and axonal integrity were significantly reduced in newly diagnosed, treatment-naïve OSA over control subjects, indicating both myelin and axonal changes. These myelin and axonal changes were localized in various brain areas critical for cardiovascular and respiratory regulation, and included medullary as well as cerebellar, basal ganglia, limbic, and corpus callosum areas, and regions within the corona radiata. Myelin changes were more widespread than axonal changes in OSA, indicating predominant myelin pathology over axonal injury, but both types of changes were preferentially left-sided; a notable exception was right-sided ventral medulla injury. Hypoxemia associated with OSA may contribute primarily to myelin changes; myelin is more vulnerable to hypoxia than axons. The acute nature of myelin and axonal changes indicates a potential for axonal tissue and functional recovery with use of myelin-repair drugs and breathing treatment in newly diagnosed OSA subjects.

ACKNOWLEDGMENTS

This research was supported by the National Instututes of Health R01 HL-113251.

DISCLOSURE STATEMENT

This was not an industry supported study. The authors have indicated no financial conflicts of interest. Study site was University of California at Los Angeles.

REFERENCES

1. Kumar R, Chavez AS, Macey PM, Woo MA, Yan-Go FL, Harper RM. Altered global and regional brain mean diffusivity in patients with obstructive sleep apnea. J Neurosci Res 2012;90:2043-52.
2. Macey PM, Kumar R, Woo MA, Valladares EM, Yan-Go FL, Harper RM. Brain structural changes in obstructive sleep apnea. Sleep 2008;31:967-77.
3. Macey PM, Henderson LA, Macey KE, et al. Brain morphology associated with obstructive sleep apnea. Am J Resp Crit Care 2002;166:1382-7.
4. Torelli F, Moscufo N, Garreffa G, et al. Cognitive profile and brain morphological changes in obstructive sleep apnea. Neuroimage 2011;54:787-93.
5. Morrell MJ, Jackson ML, Twigg GL, et al. Changes in brain morphology in patients with obstructive sleep apnoea. Thorax 2010;65:908-14.
6. Morrell MJ, McRobbie DW, Quest RA, Cummin AR, Ghiassi R, Corfield DR. Changes in brain morphology associated with obstructive sleep apnea. Sleep Med 2003;4:451-4.
7. Pantoni L, Garcia JH, Gutierrez JA. Cerebral white matter is highly vulnerable to ischemia. Stroke 1996;27:1641-6; discussion 7.
8. Kumar R, Macey PM, Woo MA, Alger JR, Harper RM. Diffusion tensor imaging demonstrates brainstem and cerebellar abnormalities in congenital central hypoventilation syndrome. Pediatr Res 2008;64:275-80.
9. Kumar R, Macey PM, Woo MA, Harper RM. Rostral brain axonal injury in congenital central hypoventilation syndrome. J Neurosci Res 2010;88:2146-54.
10. Kumar R, Woo MA, Macey PM, Fonarow GC, Hamilton MA, Harper RM. Brain axonal and myelin evaluation in heart failure. J Neurol Sci 2011;307:106-13.
11. Song SK, Sun SW, Ramsbottom MJ, Chang C, Russell J, Cross AH. Dysmyelination revealed through MRI as increased radial (but unchanged axial) diffusion of water. Neuroimage 2002;17:1429-36.
12. Song SK, Yoshino J, Le TQ, et al. Demyelination increases radial diffusivity in corpus callosum of mouse brain. Neuroimage 2005;26:132-40.
13. Blaschek A, Keeser D, Muller S, et al. Early white matter changes in childhood multiple sclerosis: a diffusion tensor imaging study. Am J Neuroradiol 2013;34:2015-20.
14. Ryan NS, Keihaninejad S, Shakespeare TJ, et al. Magnetic resonance imaging evidence for presymptomatic change in thalamus and caudate in familial Alzheimer's disease. Brain 2013;136:1399-414.
15. Betz J, Zhuo J, Roy A, Shanmuganathan K, Gullapalli RP. Prognostic value of diffusion tensor imaging parameters in severe traumatic brain injury. J Neurotrauma 2012;29:1292-305.
16. Widjaja E, Kis A, Go C, Raybaud C, Snead OC, Smith ML. Abnormal white matter on diffusion tensor imaging in children with new-onset seizures. Epilepsy Res 2013;104:105-11.
17. Kumar R, Nguyen HD, Macey PM, Woo MA, Harper RM. Regional brain axial and radial diffusivity changes during development. J Neurosci Res 2012;90:346-55.
18. Kumar R, Chavez AS, Macey PM, Woo MA, Harper RM. Brain axial and radial diffusivity changes with age and gender in healthy adults. Brain Res 2013;1512:22-36.
19. Waradekar NV, Sinoway LI, Zwillich CW, Leuenberger UA. Influence of treatment on muscle sympathetic nerve activity in sleep apnea. Am J Resp Crit Care 1996;153:1333-8.
20. Knutson KL, Rathouz PJ, Yan LL, Liu K, Lauderdale DS. Stability of the Pittsburgh Sleep Quality Index and the Epworth Sleepiness Questionnaires over 1 year in early middle-aged adults: the CARDIA study. Sleep 2006;29:1503-6.
21. Jiang H, van Zijl PC, Kim J, Pearlson GD, Mori S. DtiStudio: resource program for diffusion tensor computation and fiber bundle tracking. Comput Methods Programs Biomed 2006;81:106-16.
22. Ashburner J, Friston KJ. Unified segmentation. Neuroimage 2005;26:839-51.

23. Beaulieu C. The basis of anisotropic water diffusion in the nervous system - a technical review. NMR Biomed 2002;15:435-55.
24. Trip SA, Wheeler-Kingshott C, Jones SJ, et al. Optic nerve diffusion tensor imaging in optic neuritis. Neuroimage 2006;30:498-505.
25. Takahashi M, Ono J, Harada K, Maeda M, Hackney DB. Diffusional anisotropy in cranial nerves with maturation: quantitative evaluation with diffusion MR imaging in rats. Radiology 2000;216:881-5.
26. Budde MD, Frank JA. Neurite beading is sufficient to decrease the apparent diffusion coefficient after ischemic stroke. Proc Natl Acad Sci U S A 2010;107:14472-7.
27. Lowry OH, Passonneau JV, Hasselberger FX, Schulz DW. Effect of Ischemia on Known Substrates and Cofactors of the Glycolytic Pathway in Brain. J Biol Chem 1964;239:18-30.
28. Hossmann KA. Cortical steady potential, impedance and excitability changes during and after total ischemia of cat brain. Exp Neurol 1971;32:163-75.
29. Oehmichen M, Ochs U, Meissner C. Regional potassium distribution in the brain in forensic relevant types of intoxication preliminary morphometric evaluation using a histochemical method. Neurotoxicology 2001;22:99-107.
30. Mintorovitch J, Yang GY, Shimizu H, Kucharczyk J, Chan PH, Weinstein PR. Diffusion-weighted magnetic resonance imaging of acute focal cerebral ischemia: comparison of signal intensity with changes in brain water and Na+,K(+)-ATPase activity. J Cereb Blood Flow Metab 1994;14:332-6.
31. Benveniste H, Drejer J, Schousboe A, Diemer NH. Elevation of the extracellular concentrations of glutamate and aspartate in rat hippocampus during transient cerebral ischemia monitored by intracerebral microdialysis. J Neurochem 1984;43:1369-74.
32. Kassmann CM, Nave KA. Oligodendroglial impact on axonal function and survival - a hypothesis. Curr Opin Neurol 2008;21:235-41.
33. Shereen A, Nemkul N, Yang D, et al. Ex vivo diffusion tensor imaging and neuropathological correlation in a murine model of hypoxia-ischemia-induced thrombotic stroke. J Cereb Blood Flow Metab 2011;31:1155-69.
34. Nukada H, Dyck PJ. Acute ischemia causes axonal stasis, swelling, attenuation, and secondary demyelination. Ann Neurol 1987;22:311-8.
35. Yang Q, Tress BM, Barber PA, et al. Serial study of apparent diffusion coefficient and anisotropy in patients with acute stroke. Stroke 1999;30:2382-90.
36. Bhagat YA, Hussain MS, Stobbe RW, et al. Elevations of diffusion anisotropy are associated with hyper-acute stroke: a serial imaging study. Magn Reson Imaging 2008;26:683-93.
37. Minkner K, Lovblad KO, Yilmaz H, et al. White matter lesions in watershed territories studied with MRI and parenchymography: a comparative study. Neuroradiology 2005;47:425-30.
38. Schwartz PJ, Periti M, Malliani A. The long Q-T syndrome. Am Heart J 1975;89:378-90.
39. Rice TB, Foster GD, Sanders MH, et al. The relationship between obstructive sleep apnea and self-reported stroke or coronary heart disease in overweight and obese adults with type 2 diabetes mellitus. Sleep 2012;35:1293-8.
40. Kumar R, Birrer BV, Macey PM, et al. Reduced mammillary body volume in patients with obstructive sleep apnea. Neurosci Lett 2008;438:330-4.
41. Kumar R, Macey PM, Cross RL, Woo MA, Yan-Go FL, Harper RM. Neural alterations associated with anxiety symptoms in obstructive sleep apnea syndrome. Depress Anxiety 2009;26:480-91.
42. Cross RL, Kumar R, Macey PM, et al. Neural alterations and depressive symptoms in obstructive sleep apnea patients. Sleep 2008;31:1103-9.
43. Nattie EE, Li AH, St John WM. Lesions in retrotrapezoid nucleus decrease ventilatory output in anesthetized or decerebrate cats. J Appl Physiol 1991;71:1364-75.
44. Smith JC, Ellenberger HH, Ballanyi K, Richter DW, Feldman JL. Pre-Botzinger complex: a brainstem region that may generate respiratory rhythm in mammals. Science 1991;254:726-9.
45. Dampney RA, Horiuchi J, Tagawa T, Fontes MA, Potts PD, Polson JW. Medullary and supramedullary mechanisms regulating sympathetic vasomotor tone. Acta Physiol Scand 2003;177:209-18.
46. Dampney RA, McAllen RM. Differential control of sympathetic fibres supplying hindlimb skin and muscle by subretrofacial neurones in the cat. J Physiol 1988;395:41-56.
47. Rukhadze I, Fenik VB, Benincasa KE, Price A, Kubin L. Chronic intermittent hypoxia alters density of aminergic terminals and receptors in the hypoglossal motor nucleus. Am J Resp Crit Care 2010;182:1321-9.
48. Harper RM, Macey PM, Henderson LA, et al. fMRI responses to cold pressor challenges in control and obstructive sleep apnea subjects. J Appl Physiol 2003;94:1583-95.
49. Horiuchi J, Dampney RA. Evidence for tonic disinhibition of RVLM sympathoexcitatory neurons from the caudal pressor area. Auton Neurosci 2002;99:102-10.
50. Ogren JA, Macey PM, Kumar R, et al. Impaired cerebellar and limbic responses to the valsalva maneuver in heart failure. Cerebellum 2012;11:931-8.
51. Ogren JA, Macey PM, Kumar R, Woo MA, Harper RM. Central autonomic regulation in congenital central hypoventilation syndrome. Neuroscience 2010;167:1249-56.
52. Woo MA, Macey PM, Keens PT, et al. Aberrant central nervous system responses to the Valsalva maneuver in heart failure. Congest Heart Fail 2007;13:29-35.
53. Macey PM, Kumar R, Yan-Go FL, Woo MA, Harper RM. Sex differences in white matter alterations accompanying obstructive sleep apnea. Sleep 2012;35:1603-13.